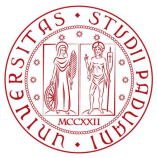

UNIVERSITÀ DEGLI STUDI DI PADOVA

DIPARTIMENTO DI FISICA E ASTRONOMIA "GALILEO GALILEI"

CORSO DI LAUREA TRIENNALE IN ASTRONOMIA

QUASARS AND THEIR HOST GALAXIES
I QUASAR E LE LORO GALASSIE OSPITI

Laureanda
VALERIA VANZANI

Relatore
PROF. MAURO D'ONOFRIO

Correlatrice
DOTT.SSA PAOLA MARZIANI

Anno Accademico 2015/2016

He wondered how he could ever have thought of planets, even of the Earth, as islands of life and reality floating in a deadly void. Now, with a certainty which never after deserted him, he saw the planets - the 'earths' he called them in his thought - as mere holes or gaps in the living heaven [...]. And yet, he thought, beyond the solar system the brightness ends. Is that the real void, the real death? Unless ... he groped for the idea ... unless visible light is also a hole or gap, a mere diminution of something else. Something that is to bright unchanging heaven as heaven is to the dark, heavy earths....

(C. S. Lewis, Out of the Silent Planet)

CONTENTS

ABSTRACT

This thesis is intended to give a general overview of one of the most forestanding research field of modern astrophysics: the quasar phenomenon. A description of the optical-UV spectroscopic properties and the spectral energy distribution is presented, followed by a discussion of the basic accretion mechanism and the different accretion modes. Then the thesis concentrates on the classification scheme of the Four-Dimensional Eigenvector 1 parameter space. The morphological properties of quasar hosts are also described. Finally, the thesis suggests a possible way to organize future morphological studies in the search for a connection between host morphology and the 4DE1 quasar sequence.

Keywords: quasars, emission lines, host galaxy, active galactic nuclei, optical and UV spectroscopy, accretion disks.

CHAPTER 1

INTRODUCTION: LOW REDSHIFT QUASARS IN THE CONTEXT OF AGN UNIFICATION

A quasar is a high luminosity active galactic nucleus (AGN) that shows an intense optical-UV continuum, X-ray emission and strongly broadened emission lines in the optical spectrum; this great energy production is caused by accretion of gas onto a supermassive black hole in the nucleus of a galaxy. At the beginning of their observations in the early 1960s, these sources were called 'quasi stellar radio sources' (then abbreviated as 'quasars') because in optical images they appear as pointlike counterparts of radio sources: at that time, the host galaxy was too faint to be detected compared with the bright glare of the nucleus.
AGN are first divided into two types: type I optical spectra show both broad (> 1000 km/s up to 20 000 km/s) and narrow (< 1000 km/s) emission lines, and bright and variable continua; type II spectra show only narrow emission lines and a weak and nearly constant continuum. Classicaly, quasars represent type I AGN at high luminosity, while at low luminosity the host galaxy is well visible and the source is called Seyfert I galaxy (the absolute magnitude boundary between Seyfert galaxies and quasars is $M_B = -22.2$ with $H_0 = 70$ km s^{-1} Mpc^{-1}, $\Omega_m = 0.3$ and $\Omega_\Lambda = 0.7$. The same cosmology will be assumed throughout this thesis).
The difference between type I and II AGN is explained with a model composed of a flattened gas distribution related to the accretion disk from which broad line emission arises (Broad Line Region BLR), plus an obscuring torus of molecular gas. If the source is seen nearly edge-on, the torus obscures the broad line emission from the accretion disk and the continuum (type II), while if it is seen from intermediate angles up to nearly face-on there is no obscuration (type I). Narrow lines can instead be seen at almost all orientations because they originate from a lower density gas that extends above and below the torus, in a region that is farther away from the accretion disk (Narrow Line Region NLR) (Antonucci 1993, Chapter 7 of Netzer 2013). Morphology of the host galaxy and environment could also play an important role in the difference between type I and type II quasars (this part will not be discussed in this thesis, see instead Dultzin-Hacyan et al. 1999 and Villarroel & Korn 2014).
The majority of quasars are radio-quiet (RQ), but a small fraction (8%) is found to be radio-loud (RL), meaning that they also show a strong emission in radio wavelengths. A precise and unique criterion to discriminate between RQ and RL is still missing. A traditional and commonly used criterion is the one proposed by Kellermann et al. (1989) for luminous quasars (absolute magnitude in B-band $M_B \approx -26$): a quasar is considered radio-loud if the ratio R_K of the monochromatic luminosities at 5 GHz (radio) over B-band (optical) is greater than 10. However, following studies found out that R_K is luminosity-dependent, so the fixed boundary set at $R_K = 10$ is not valid for

lower luminosity sources: it is better to use $R_K \propto L^{-0.5}$ (Laor 2003). Recently, Zamfir et al. (2008) proposed a new criterion based on radio morphology and orientation considerations: a radio-loud quasar shows a radio luminosity at 1.4 GHz $L_{1.4GHz} \geq 10^{31.6}$ $erg\ s^{-1}\ Hz^{-1}$, which is a more restrictive boundary because it corresponds to about $R_K > 70$.

Radio-loud quasars can have a lobe-dominated radio structure, or a core-dominated or intermediate core-jet structure. Lobe-dominated radio sources are usually divided into two types (from Fanaroff-Riley classification, Fanaroff & Riley 1974): FR I sources show a radio brightness that decreases following the jets away from the core; instead, in FR II type, the radio brightness increases towards the extremes of the jets (hot spots). Radio-loud quasars are now found in both types, although a double-lobed FR II structure appears to be the most common type (Zamfir et al. 2008).

Thanks to their high luminosity (bolometric luminosity L_{bol} in the range $10^{44} - 10^{48}$ erg/s), quasars can be seen up to great distances in the Universe: from redshift $z = 0.16$ of 3C 273, one of the first discovered, to the most distant now at $z = 7.085$. However, in order to understand well their structure and the morphological properties of their hosts, it is better to concentrate on low redshift quasars ($z < 1$ or below, depending on the type of study). Luckily, since the basic mechanism is always accretion onto a supermassive black hole, independently of L and z, a part of the results for spectroscopic and morphological properties of low-z quasars can be extended also to high-z ones (Sulentic et al. 2000, Falomo et al. 2014).

The study of both AGN features and host galaxy properties is important in order to understand the role of AGN activity in the early stages of galaxy evolution. Chapter 2 describes first the optical-UV spectroscopic properties and then the general spectral energy distribution for low redshift quasars. Chapter 3 concentrates on the accretion mechanism that powers AGN. Chapter 4 discusses a possible way to organize the great variety of spectroscopic features thanks to a scheme called 4DE1 (Four-Dimensional Eigenvector 1). Particular attention is dedicated to the morphological properties of host galaxies in Chapter 5. Finally, Chapter 6 describes a possible future perspective to improve the understanding of quasars, and Chapter 7 summarizes the discussion.

CHAPTER 2

GENERAL PROPERTIES OF QUASAR SPECTRA

2.1 OPTICAL-UV SPECTROSCOPIC PROPERTIES

A typical quasar spectrum in the optical-UV domain shows a bright continuum and both broad and narrow emission lines from various elements at different ionization levels: for example, several blends of FeII lines, hydrogen lines from Balmer and Lyman series, HeI and HeII, C III and C IV, Mg II, O II and O III and other lines. The intensity of the optical-UV continuum shows a variability on a timescale of the order of weeks-months: this fact implies that this great energy production arises from a small-size region, of the order of a light-month or less.
Fig. 2.1 shows a composite spectrum in the near-UV and optical ranges, obtained from about 2200 individual spectra of SDSS (Sloan Digital Sky Survey) of different redshift and luminosity. The intensity of the continuum increases moving towards shorter wavelengths in the so-called Big Blue Bump, consistent with the predictions of the standard accretion disk model (see Chapter 3). Emission lines appear over most of the continuum, frequently in blends of stronger and fainter lines. Starting from the UV part of the spectrum, some of the strongest lines are $Ly\alpha$ λ1215, C IV λ1549, Mg II λ2800, $H\beta$ λ4862, [O III] $\lambda\lambda 4959, 5007$ (narrow forbidden lines), and $H\alpha$ λ6563 with the close lines of [N II] $\lambda\lambda 6548, 6583$. Strong blends from Fe II multiplets are also present, in particular in the region between 2200-4000 Å, at 4570 Å and at 5130 Å.

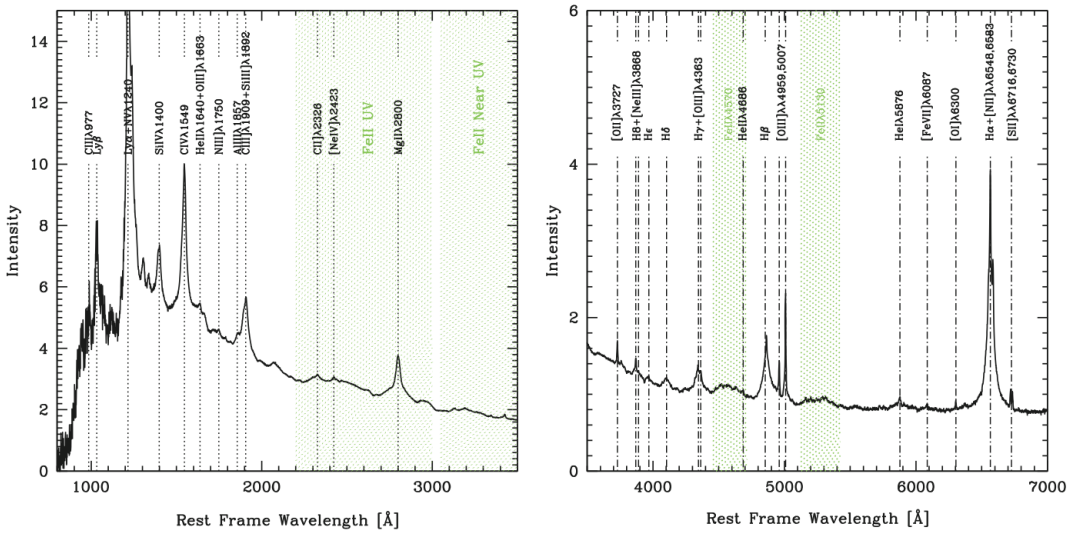

Figure 2.1: Quasar composite spectrum from SDSS in the near-UV (left) and optical (right) domains. The most important emission lines are indicated. Shaded areas correspond to Fe II blends (Chapter 3 of D'Onofrio et al. 2012).

The broad ($> 1000\ km/s$) permitted lines are usually stronger than the corresponding narrow ($< 1000\ km/s$) forbidden lines.The BLR from which broad lines originate is thought to be a high-density gas located at some light-months (or about 0.1 pc) from the central BH. The gas is photo-ionized by the accretion disk continuum and is under the influence of the black hole potential, so that the line FWHM can give an estimate of the BH mass. Instead, narrow lines are produced in a lower-density ($\approx 10^4\ cm^{-3}$) gas that extends farther away (up to kpc distances) from the accretion disk, and, in a first approximation, they give an estimate of the local quasar rest frame. The NLR can be resolved in nearby quasars, while the BLR is still always too small to be resolved. A schematic representation of the location and scale of these components is shown in Figs. 2.4 and 3.1.

It is convenient to separate broad lines in high-ionization (HIL, for example the C IV line at 1549 Å) and low-ionization lines (LIL, for example the $H\beta$ Balmer line and the blend of Fe II lines at 4570 Å), because they are thought to arise from different parts of the BLR. For low ionization broad lines, it is not yet clear whether they originate from the outer part of the accretion disk, or from an optically thick and flattened distribution of clouds related to the disk. In any case, the density of the medium must be much higher than $10^9\ cm^{-3}$ in order to account for the Fe II emission (Sulentic et al. 2000). Instead, high ionization broad lines may be related to an optically thin outflow, an accretion disk wind, in particular in the high-accreting quasars (Collin-Souffrin & Lasota 1988, Chapter 6 of D'Onofrio et al. 2012).

Fig. 2.2 shows a possible geometrical configuration of the BLR, with Fe II emission arising from the outer part of the accretion disk, $H\beta$ emitting clouds in a flattened distribution that is gravitationally bound to the disk, and C IV emitting gas outflowing in clouds above the disk. In this configuration, apart from the intrinsic diversity, the features of the emission lines vary depending on orientation: if the source is observed

face-on, it shows narrower $H\beta$ and stronger Fe II lines; broader $H\beta$ and weaker Fe II lines if it is oriented near edge-on.
Broad lines can show centroid shifts with respect to the quasar rest frame and asymmetries with respect to the line peak. The most evident effect is the blueshift of the high ionization lines in high-accreting quasars (population A, see Chapter 4), in particular in the C IV line at 1549 Å. This blueshift has been interpreted as a hint of a 'radiation line-driven' wind: UV photons from the continuum excite the atoms in the atmosphere of the accretion disk and blow them out in an outflow (Proga et al. 2000). This process can happen only until the atoms are not completely ionized by the higher-energy photons of the X-ray continuum. Indeed, sources with strong HIL blueshifts (and so a strong wind component) are found to have a weaker flux in the X-ray domain compared to UV flux; while quasars with a stronger X-ray continuum show little or no blueshift, and so probably they do not have a dominant wind component (Marziani et al. 1996, Richards et al. 2011).
In addition to the diversity in the C IV line shift, different functions are used to fit the broad line profiles. In particular, for the $H\beta$ Balmer line, the best fitting is obtained with an almost symmetric Lorentzian function if $FWHM < 4000\ km/s$, and with a red asymmetric double Gaussian model if $FWHM > 4000\ km/s$. The differences in C IV and Balmer line profiles are explained with the distinction of two different quasar populations, respectively called population A if $FWHM < 4000\ km/s$, and population B if $FWHM > 4000\ km/s$ (an appropriate discussion is presented in Chapter 4).

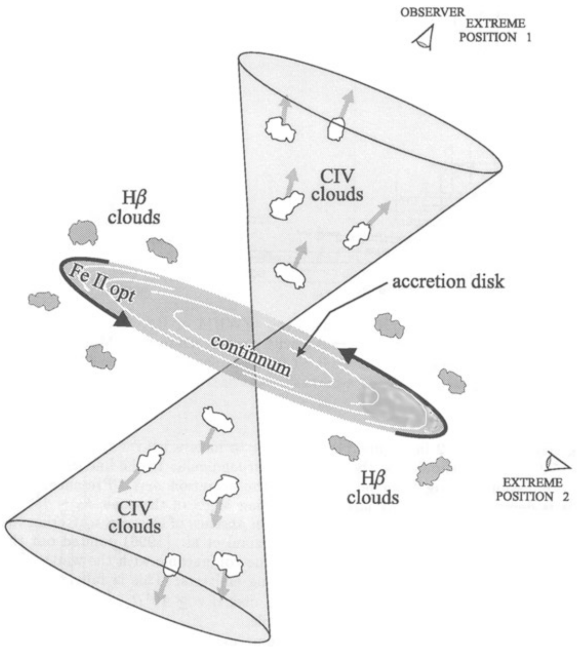

Figure 2.2: Possible geometrical configuration of the BLR, in case of a large enough accretion rate able to produce a disk wind (Chapter 5 of D'Onofrio et al. 2012).

2.2 MULTI-WAVELENGTH SPECTRAL ENERGY DISTRIBUTION

Quasars have a rich spectral energy distribution that ranges from radio wavelengths to gamma rays, and the study of their properties in all the domains of the electromagnetic spectrum is important in order to obtain a better understanding of their structure and evolution. In fact, many distinctions of different AGN classes, for example type I and type II, or population A and B, or radio-loud and radio-quiet, are based on the different features showed in various part of the electromagnetic spectrum. The discussion presented in this section is based on Chapters 3 and 6 of D'Onofrio et al. 2012 and Chapters 1 and 7 of Netzer 2013.
In general, the optical-UV-X-ray domain is dominated by thermal emission, while at the radio and gamma-ray wavelenghts, very different in radio-loud and radio-quiet quasars, the emission is nonthermal. In almost all wavelengths, the emission is variable with timescales that range from weeks in the optical domain to minutes at the highest energies. Fig. 2.3 shows the typical SED of a radio-quiet quasar, together with the main components that will be described in the next paragraphs. In the infrared-optical-UV domain, the emission is fitted with a model composed of an accretion disk with the peak in the UV, and an obscuring dusty torus emitting mainly in the infrared. The X-ray domain involves the soft excess, the emission from the disk corona and the disk reflection of external radiation. The radio energy distribution is a synchrotron power law of lower intensity. The difference between RQ and RL sources is evident from the radio-loud SED shown at cm wavelenghts.

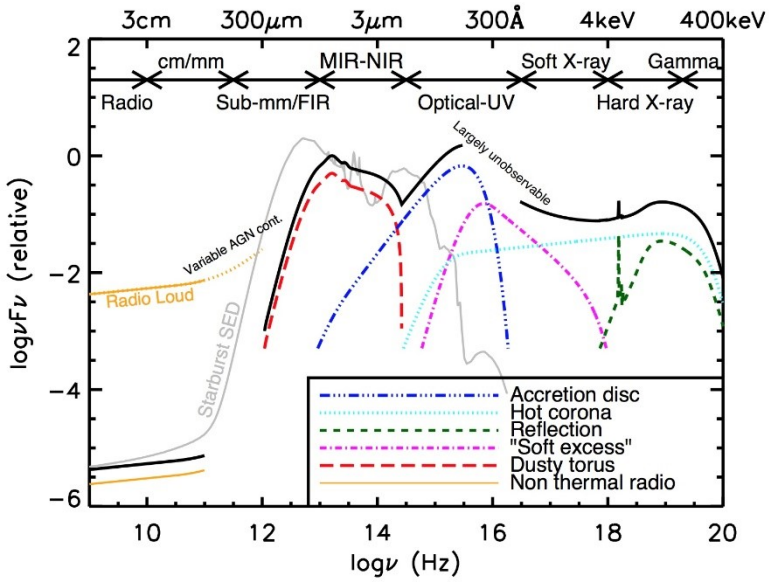

Figure 2.3: Schematic representation of a radio-quiet quasar SED. The black solid curve is the total observed energy distribution, the coloured curves show the different components. The radio emission in the case of a radio-loud quasar (orange line) and the SED of a starburst galaxy (grey curve) are also shown for comparison (http://astro.dur.ac.uk/ cpnc25/research.html).

Radio wavelenghts The radio emission is mainly related to nonthermal radiation from jets (collimated outflows) caused by synchrotron process, that is the emission of radiation by relativistic electrons in a magnetic field. Jets are believed to arise from very near the BH event horizon, due to a relativistic mechanism that requires a rotating black hole and very strong magnetic fields associated with the accretion disk. Jets likely become relativistic and highly collimated within a few thousand times the BH gravitational radius (Chapter 6 of D'Onofrio et al. 2012), and may extend up to kpc distances if they can proceed throughout the interstellar medium.
A radio emission is present in all quasars, but in the majority of radio-quiet sources only a weak radio emission and scarcely defined jets are detected.
Radio-loud quasars show a power-law spectrum: the monochromatic flux depends on the frequency with a relation $F_\nu \propto \nu^{-\alpha_R}$.
Sources with $\alpha_R < 0.5$ are called flat-spectrum and correspond to core-dominated RL quasars, while sources with $\alpha_R > 0.5$ are said steep-spectrum and correspond to a lobe-dominated radio morphology, usually FR II. This fact can be explained by assuming that FR II is the parent population of RL quasars and that the radio jet is perpendicular to the accretion disk, so when the source is viewed nearly face-on (near the radio jet axis), it appears as core-dominated and more radio luminous (because of relativistic beaming). Instead, at intermediate angles, a less radio luminous lobe-dominated quasar is observed. This also means that the radio luminosity of the weakest FR II can be considered the minimum limit of radio luminosity for all RL quasars, defining a boundary between RQ and RL sources. As mentioned in Chapter 1, this limit appears to be at $L_{1.4GHz} \approx 10^{31.6}\ erg\ s^{-1}\ Hz^{-1}$.

Infrared wavelenghts The quasar energy distribution shows a minimum at about $1\mu m$: at this wavelength, the optical continuum declines and the infrared emission from dust begins. Indeed, with the exception of a minority of radio-loud quasars dominated by synchrotron emission also at infrared wavelengths, the emission in this band is mainly due to circumnuclear dust that absorbs the radiation from the central source and re-radiates away the energy as a thermal emission. This thermal emission peaks between $1 - 30\mu m$, which corresponds to a blackbody temperature of the order of $100 - 1000\ K$ (Chapter 1 of Netzer 2013).
The infrared emission has been interpreted as an evidence of the presence of a thick torus of molecular gas and dust, extended between about $1 - 100\ pc$ from the central BH, as proposed in the AGN unification model (see Figs. 2.4 and 3.1). In fact, type II AGN, that are believed to be obscured quasars and show a weak optical continuum, have a more intense emission at infrared wavelengths, especially in the far infrared (Gruppioni et al. 2016, and references therein).

X-ray domain The power emitted in X-ray wavelengths represents about $1-10\%$ of the total bolometric power of a quasar, with high-luminosity quasars as weaker X-ray emitters; moreover, the emission is slight more intense for radio-loud sources compared to radio-quiet.
At a first approximation, the spectral energy distribution between 1-100 keV (10-0.1 Å, hard X-rays) can be described with a power-law function $L_\nu \propto \nu^{-\alpha}$, with a drop

after 100 keV. This emission is thought to be caused by the hot corona of the accretion disk (see Chapter 3). The drop at high energies depends on the corona temperature ($T \geq 10^7$ K). The size of this region is likely to be very small, of the order of some light-hours, because of the short variability timescale observed at the X-ray domain.
The photon index Γ is commonly used in order to describe the strength of the emission in a certain X-ray range of energy. It is the index that describes the relation between $N(E)$, the number of emitted photons per unit time and energy, and the energy E: $N(E) \propto E^{-\Gamma}$. The photon index is related to the power-law spectral index α simply by $\Gamma = \alpha + 1$:

$$L_E dE = L_\nu d\nu \propto \nu^{-\alpha} d\nu \propto \left(\frac{E}{h}\right)^{-\alpha} \frac{dE}{h} \implies L_E \propto E^{-\alpha} \implies N(E) \propto \frac{L_E}{E} \propto E^{-\alpha-1} \tag{2.1}$$

where $E = h\nu$ is the energy of a photon of frequency ν and h is Planck constant. In many cases, in the hard X-ray domain $\alpha_{hard} \approx 1$ and $\Gamma_{hard} \approx 2$.
In the soft X-ray range (below 1 keV) the spectrum rises above the power-law function that represents the energy distribution in the hard X-ray domain: it is the so-called 'soft X-ray excess'. The excess emission could come directly from the accretion disk, or from reflection of the external radiation from the corona. This feature is particularly evident in population A quasars, with a median value $\Gamma_{soft} \approx 2.4$, while population B sources have $\Gamma_{soft} \approx 2.0$, consistent with no significant soft X-ray excess above the hard X-ray power law (Bensch et al. 2015, and references therein).

Gamma-ray domain The majority of quasars do not show a significant emission in the gamma-ray range, with the exception of the blazar class, which appears to be gamma-ray-loud up to about 300 GeV. Blazars are core-dominated radio-loud sources that show a highly variable (on minutes-hours timescales) and polarized emission in both the radio and gamma-ray domains: the common interpretation is that they are radio-loud quasars in which the relativistic jet is viewed almost face-on (see Fig. 2.4) (Ghisellini & Tavecchio 2009, Chapter 6 of Netzer 2013).
The emission in these sources is dominated by synchrotron radiation from radio to UV wavelengths, while in the X-ray and gamma-ray domains it is due to inverse Compton effect: relativistic electrons transfer energy to photons which are boosted to the higher energies of gamma-rays. These photons can come either from the same relativistic particles producing synchrotron radiation (synchrotron self-Compton process) or from external sources, such as the accretion disk, the BLR or the thick torus (external Compton process).
Recently, an intense gamma-ray emission has also been detected from several Narrow-Line Seyfert I galaxies which also include the extreme of the high-accreting sources of population A (see Section 5.4).

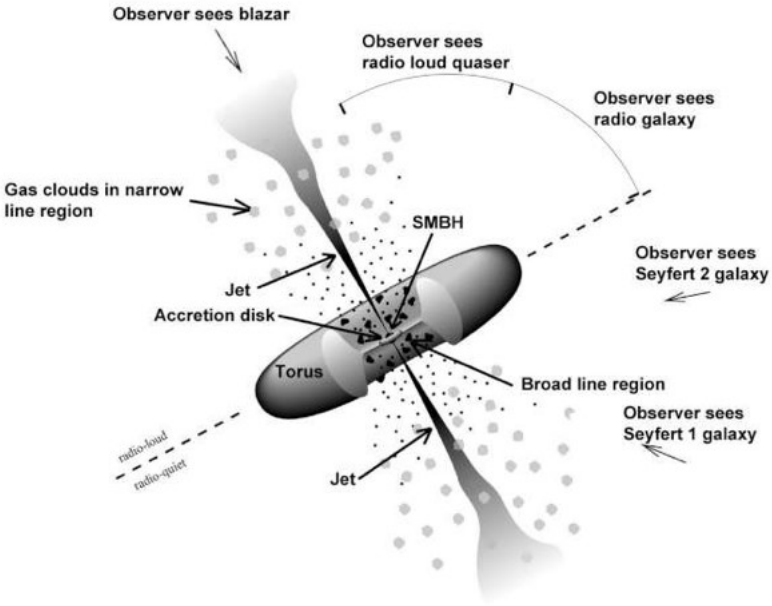

Figure 2.4: Schematic representation of the unification model for AGN. The main components described in Chapter 2 are present: the accretion disk and the BLR, the obscuring torus, the NLR clouds and the relativistic jets in case of a radio-loud source. A radio-quiet AGN is observed as a Seyfert II galaxy in a nearly edge-on orientation, while it appears as a Seyfert I galaxy or as a luminous RQ quasar if unobscured. A radio-loud AGN appears as a radio galaxy, a RL quasar or a blazar while moving from edge-on to face-on orientation (http://fermi.gsfc.nasa.gov/).

CHAPTER 3

INTERPRETATION OF OBSERVATIONS ON THE BASIS OF THE STANDARD ACCRETION MODEL

The principal source that powers active galactic nuclei and produces the observed spectra is an accretion disk of gas that is spiraling towards the central black hole. However, some systematic differences observed in AGN spectra may hint at different accretion disk modes. Following the discussion in Chapters 3-4 of Netzer 2013, accretion disks can be geometrically thin, slim or thick depending on their shape, which is eventually determined by the value of the accretion rate. Also the BH mass and spin can influence the disk properties. In particular, the accretion rate determines the temperature of the disk, and so the relative importance of radiation pressure and gas pressure. Each geometrical type can then be optically thin or thick depending on the surface density and the ionization level.
The accretion rate $\dot{M}$ is given by the bolometric luminosity L_{bol} and the mass-to-luminosity conversion efficiency η:

$$\dot{M} = \frac{L_{bol}}{\eta \cdot c^2} \tag{3.1}$$

where η depends on BH properties such as its spin parameter a; for a Schwarzschild black hole, $a = 0$ and $\eta \approx 0.057$.
The Eddington accretion rate $\dot{M}_{edd}$ is the accretion rate associated with Eddington Luminosity L_{edd}, and L_{edd} is related to the black hole mass M_{BH}:

$$L_{edd} \approx 1.28 \cdot 10^{38} \cdot \frac{M_{BH}}{M_\odot} erg/s \tag{3.2}$$

for a pure hydrogen gas.
The dimensionless accretion rate is given by:

$$\frac{\dot{M}}{\dot{M}_{edd}} = \frac{L_{bol}/\eta(\dot{M}, a)c^2}{L_{edd}/\eta(\dot{M}_{edd}, a)c^2} = \frac{L_{bol}}{L_{edd}} \cdot \frac{\eta(\dot{M}, a)}{\eta(\dot{M}_{edd}, a)} \tag{3.3}$$

The Eddington ratio L_{bol}/L_{edd}, which can be determined from observations, could be used in place of the dimensionless accretion rate only whether η were a constant. However, η depends on the BH spin parameter a and the accretion rate $\dot{M}$, and in particular tends to decrease for high $\dot{M}$ values.

3.1 THE STANDARD THIN DISK AND THE DISK CORONA

The first simplified standard model used to explain quasar spectra is the geometrically thin and optically thick accretion disk, which is valid for an Eddington ratio in the

range $0.01 \lesssim L_{bol}/L_{edd} \lesssim 0.3$ and implies a ratio of thickness over radius $h/r \ll 0.1$ (this is why 'geometrically thin').
The basic assumptions of this model are:

- The disk is in a stationary state, the gas density and the disk height are time-independent;
- The accreted gas moves inward very slowly retaining almost a circular Keplerian motion (with a radial velocity much smaller than the Keplerian velocity), so inflowing in a tight spiral;
- The motion of each gas ring is subject to a viscosity torque due to the motion of the other gas particles inside the ring; the viscosity mainly depends on turbulence and magnetic fields;
- The gas inside the radius r_{in} of the innermost stable circular orbit [1] falls directly towards the center with a non-circular motion, and exerts no viscosity torque on the external disk.

While moving inward, the gas loses gravitational energy, which is converted with high efficiency into electromagnetic radiation. The disk is efficiently cooled by radiation, because the gas inflow is slow and so its timescale is longer than the time the photons need to reach the surface. Such a disk structure is extended from the radius of the innermost stable circular orbit up to about 1000 times the BH gravitational radius (less than a light-month in the case of quasars, see Fig. 3.1 for the scale of quasar components): after this limit, the disk becomes gravitationally unstable and may give rise to gas clouds which could be part of the BLR.
Assuming the local emission at each radius as a blackbody emission, the maximum temperature reached at the inner boundary r_{in} of the disk is $T \approx 10^5\ K$ for a BH mass of $10^8\ M_\odot$: this results in a peak at UV wavelengths, which is indeed what is observed in a typical quasar spectrum at a first simplified glance.

However, in real accretion disks, strong magnetic fields and a vertical density gradient can increase the contribution of viscosity and turbulence, and so can bring to an expansion and temperature rise of the outer layers. This results in the formation of an optically thin corona with a temperature $T > 10^7\ K$, which upscatters the photons emitted by the disk to hard X-ray wavelengths, through Comptonization [2] and free-free processes. The corona component can explain the hard X-ray emission of many quasars, except for the sources with the highest accretion rates that need to be treated with a different disk model.

[1] The radius r_{in} of the innermost stable circular orbit is the radius beyond which a particle falls directly into the black hole event horizon. For a stationary Schwarzschild black hole of mass M, $r_{in} = 6r_g$, where $r_g = GM/c^2$ is the gravitational radius. If the BH mass is $10^8\ M_\odot$, $r_g \approx 1.5 \cdot 10^8\ km \approx 8$ light-minutes.

[2] The Compton effect refers to the process of photon scattering by an electron, where the photon loses a certain amount of energy and so is down-scattered to a lower frequency. In the inverse Compton scattering, instead, the electron has more energy and so up-scatters the photon to a higher frequency. Comptonization refers to the change in the radiation spectrum due to these scattering processes, through which photons and electrons reach a state of equilibrium.

3.2 THE SLIM/THICK DISK AND ADVECTION-DOMINATED ACCRETION FLOWS

If the Eddington ratio exceeds the limit of about $L_{bol}/L_{edd} \approx 0.3$, an important change in the disk structure occur. The inflow timescale becomes shorter than the time the radiation needs to reach the surface: so the photons are trapped in the inflow, and the accretion disk cannot radiate away the released gravitational energy, which is instead advected towards the center with the inflowing gas. As a result, the accretion disk heats up, the temperature rise leads to a radiation pressure rise which eventually increases the thickness of the disk. The geometrically thin model is no longer valid, and a slim disk appears (thick disk if the Eddington ratio is even higher): this is thought to be the case of the high-accreting quasars (population A, see Chapter 4).
These disks cannot cool efficiently through radiation and are said to be advection-dominated accretion flows. Thick disks are no longer flattened: instead, their shape is similar to a torus with two funnels, whose walls have a high temperature, along the rotation axis. If the source is observed at an angle close to the axis, the funnel collimates the radiation and the spectrum appears dominated by a hard X-ray emission.
Advection-dominated flows can also form in the case of a very low accretion rate ($L_{bol}/L_{edd} < 0.01$). In particular, some low-luminosity AGN spectra can be explained with an accretion disk similar to the standard geometrically thin model in the outer regions, while the inner parts become thicker because the disk gas has a very low density due to the low accretion rate and is not efficiently cooled by radiation.

3.3 BLACK HOLE MASS ESTIMATION

The black hole mass of a quasar can be estimated assuming that the BLR gas rotates in Keplerian orbits only under the influence of central BH. If the centripetal acceleration is due to the gravitational force of the central mass, from the virial theorem:

$$M_{BH} = f \cdot \frac{r_{BLR} \cdot v^2}{G} \tag{3.4}$$

where G is the universal gravitational constant, v is a measure of the gas orbital velocity at r_{BLR} (usually the line FWHM), and f is a dimensionless factors that depends on the particular geometry and kinematics of the BLR. The assumption of a Keplerian motion is valid for the low ionization gas; instead the high ionization broad lines may be related to an outflow, and therefore their FWHM is less reliable in estimating M_{BH}.
r_{BLR} is estimated with the reverberation mapping method. This technique is based on the fact that a variation in the intensity of the accretion disk continuum is followed by a variation in the intensity of the broad emission line flux, with a time delay Δt that depends on the distance of the line-emitting gas from the continuum source. Then simply $r_{BLR} = c \cdot \Delta t$, where c is the speed of light. This method assumes that the BLR structure does not change over the time the light needs to travel across the region, and that the continuum-emitting region is smaller than the line-emitting region. Another assumption is a direct relationship between the observed continuum and the continuum

that drives the emission-line variations (Chapter 7 of Netzer 2013).
The reverberation mapping technique was applied to about 40 AGNs of different luminosity at low redshift ($z \leq 0.4$), which were monitored for several years in order to obtain the time delay measurements from the analysis of their optical spectra. The time delay appeared to be correlated with the quasar optical luminosity in a certain band, with a relation:

$$r_{BLR} \propto (\lambda L_\lambda)^a \tag{3.5}$$

with an exponent a in the range 0.5-0.7 (0.52 the most reliable value) and L_λ the monochromatic luminosity at 5100 Å for the $H\beta$ line. This relation mainly holds for $10^{43}\ erg/s \leq L_\lambda \leq 10^{45}\ erg/s$, while at higher and lower luminosity it is more uncertain (Marziani & Sulentic 2012, and references therein). The relation has been calibrated for the low redshift quasar sample, so that it can be used to estimate r_{BLR} for other AGNs.
The factor f takes into account the relation between the observed FWHM and the real Keplerian velocity. It depends on the particular distribution and inclination of the orbits to the line of sight, and therefore it is difficult to obtain because there is no clear model for the BLR structure and geometry so far. Actually, f is estimated applying the M_{BH}-σ relation (between the BH mass and the stellar velocity dispersion in the bulge of a galaxy) to a sample of low redshift active galaxies for which σ can be measured and reverberation mapping method gives a reliable r_{BLR} value. However, assuming the same typical value of f for all quasars is a great source of uncertainty, because the factor likely depends on the line profile shape and on the contribution of the radiation force, and therefore on the Eddington ratio. In particular, f appears to increase from low L_{bol}/L_{edd} sources towards high L_{bol}/L_{edd} ones (Marziani & Sulentic 2012).
Using the relations (3.4) and (3.5), an expression that relates M_{BH} to the FWHM of a certain broad line and the luminosity in a certain band can be calculated. For example, for $H\beta$ line and the luminosity at 5100 Å:

$$\frac{M_{BH}}{M_\odot} = 1.05 \cdot 10^8 \cdot \Big(\frac{L_{5100}}{10^{46} erg/s}\Big)^{0.65} \cdot \Big(\frac{FWHM(H\beta)}{10^3 km/s}\Big)^2 \tag{3.6}$$

The BH masses of AGNs vary from 10^5 to $10^{10}\ M_\odot$, with the majority of quasar M_{BH} in the range 10^7-$10^{9.7}\ M_\odot$.

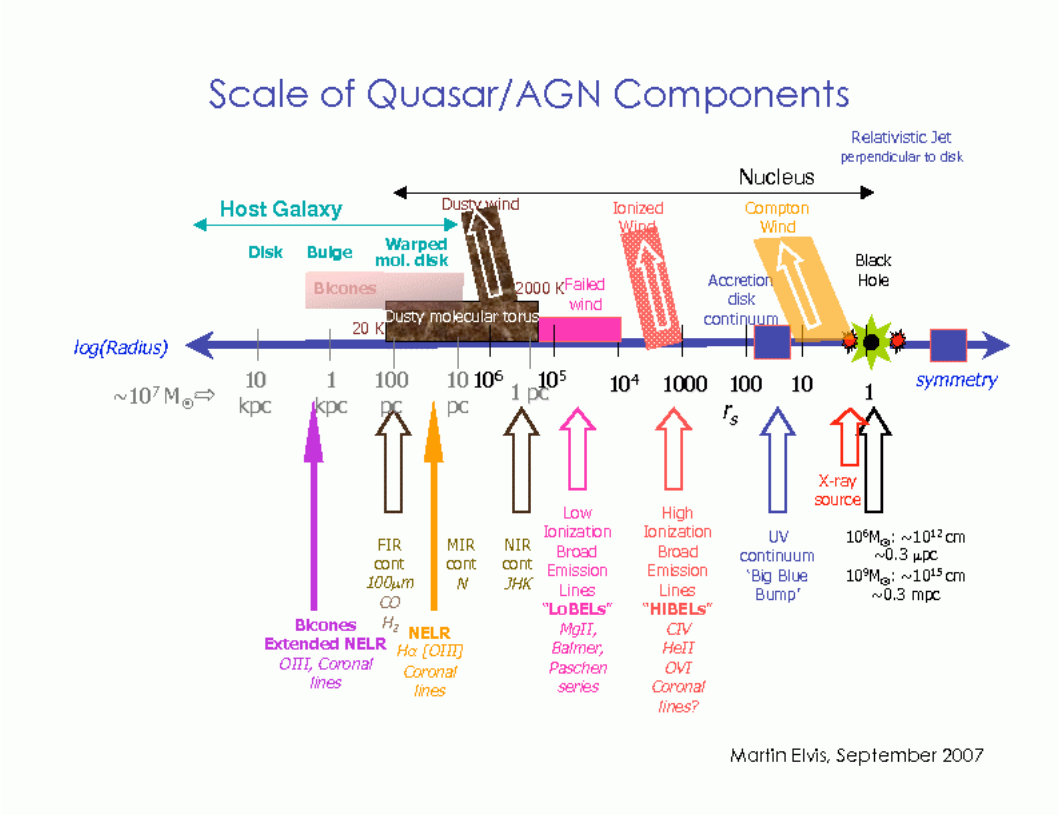

Figure 3.1: Scale of the quasar components that produce the different types of emission described in Chapters 2-3. The BH event horizon is located at 2 times the gravitational radius r_g for a Schwarzschild black hole (about 16 light-minutes for $M_{BH} \approx 10^8\ M_\odot$). The magnetic field and the BH spin drive the relativistic jet from near the event horizon, in a direction that is perpendicular to the accretion disk. The X-ray emission probably arises from the accretion disk corona on a size of about a few tens r_g. Most of the accretion disk continuum is thought to be produced in the region located at about 10-100 r_g. At $\approx$ 1000 r_g (less than a light-month) the disk becomes unstable and forms clouds which may contribute to BLR emission. The high ionization wind and the low ionization emission, maybe related to a failed wind, come from the region 100-1000r_g. The BLR may extend up to about 10^5 r_g, or 0.1-1 pc from the central black hole. Then, the dusty torus, emitting mainly in the infrared, occupies the range of distances 1-100 pc. The NLR could extend from about 10-100 pc outward in the host galaxy, reaching kpc distances in the case of an Extended NLR (http://hea-www.harvard.edu/~elvis/).

CHAPTER 4

FROM SPECTROSCOPIC ANALYSIS TO A 'QUASAR MAIN SEQUENCE'

4.1 4DE1 PARAMETER SPACE, POPULATIONS A AND B

Quasar spectra show a great variety of features, which can be due both to intrinsic diversity and to orientation effects. This chapter will focus on the spectroscopic features of type I AGN that are not obscured by the torus and therefore offer an unimpeded view of the BLR properties. It is necessary a contextualisation scheme in order to understand which are the fundamental parameters and the correlations among quasars, and whether different classes or populations can be distinguished. In this sense, one of the main interpretation scheme is the Four-Dimensional Eigenvector 1 (4DE1) parameter space, that has been defined through an advanced analysis technique called Principal Component Analysis (PCA) applied to 87 sources of the Palomar Bright Quasar survey. This and following studies found out the principal correlation (Eigenvector 1) between quasar spectroscopic parameters.
The first two fundamental parameters of 4DE1 are related to two important low ionization broad lines: $H\beta$ Balmer line and the blend of Fe II lines at 4570 Å. The optical plane of 4DE1 is obtained plotting $FWHM(H\beta)$ against the ratio R_{FeII} of equivalent width of Fe II over $H\beta$. It is easy to note that:

- Sources with large R_{FeII} usually prefer small value of $FWHM(H\beta)$ (< 4000 km/s);
- Sources with larger $FWHM(H\beta)$ (> 4000 km/s) tends to prefer smaller values of R_{FeII} (< 0.5);
- Almost all radio-loud quasars are located in the region with $R < 0.5$, with a preference for large $FWHM(H\beta)$ values (see Fig. 4.3 left panel).

The optical parameters $FWHM(H\beta)$ and R_{FeII} represent a small part of quasar spectroscopic variety and other dimensions are needed to have a better representation of the active engine. The other two parameters suggested in the 4DE1 diagram are the soft X-ray photon index and the centroid shift (relative to the rest frame as estimated from narrow lines) at half maximum of C IV broad line at 1549 Å (a high ionization broad line). Sources with a small $FWHM(H\beta)$ tend to show a large soft X-ray photon index and higher C IV blueshifts, as shown in Fig. 4.3 (right panel).
As mentioned in Chapter 2, $FWHM(H\beta)$ is usually interpreted as due to the Keplerian rotation of the BLR gas and can then stand as an estimator of BH mass. The parameter R_{FeII} can indicate the high density of the low ionization gas, because Fe II lines are more likely to be produced at electron density $n_e \gg 10^9$ cm^{-3} (Joly et al.

2008). A high soft X-ray photon index can be related to a high accretion rate. Finally, high ionization broad line blueshifts reveal the presence of a wind or outflow from the accretion disk.
The differences in the spectroscopic properties between the two extremes of the sequence in the 4DE1 diagram have suggested the distinction of two quasar populations A and B, with boundary given by $FWHM(H\beta) = 4000\ km/s$. Population A shows:

- Intense soft X-ray excess;
- Smaller $FWHM(H\beta)$ ($< 4000\ km/s$);
- Low ionization line profiles best described by Lorentzian function, usually symmetric, with blueshifts both at the line base (at 1/4 of the intensity) and peak (9/10 of the intensity) (Zamfir et al. 2009, see Fig. 4.2);
- Stronger Fe II emission (higher electron density in the BLR gas);
- Blueshifted high ionization broad lines (presence of a disk wind component, see Fig. 4.4).

The main features of population B instead are:

- No soft X-ray excess;
- Higher $FWHM(H\beta)$ ($> 4000\ km/s$);
- Low ionization line profiles best described by a double Gaussian model with an unshifted broad component of $FWHM \approx 5000\ km/s$ and a very broad component of $FWHM \approx 10\ 000\ km/s$ that is redshifted $\approx$ 1000-2000 km/s; the line profiles also show red asymmetries, redshifted line bases and blueshifted peaks (Zamfir et al. 2009, see Fig. 4.2);
- Weaker Fe II emission (lower electron density in the BLR gas);
- Unshifted high ionization broad lines (negligible or absent disk wind component, see Fig. 4.4).

The region occupied by populations A and B in the 4DE1 optical plane can be further divided into quadrants limiting the values of $FWHM(H\beta)$ and R_{FeII}, obtaining the quasar spectral types. The designations A and B are accompanied by a number that indicates the strength of Fe II emission, and by a '+' symbol representing a larger $FWHM(H\beta)$. Fig. 4.1 (left panel) represents the main spectral types that can be distinguished. Population A is divided into $A1$ ($0.0 < R_{FeII} < 0.5$), $A2$ ($0.5 < R_{FeII} < 1.0$), $A3$ ($1.0 < R_{FeII} < 1.5$) and $A4$ ($1.5 < R_{FeII} < 2.0$). Instead population B includes $B1$ ($4000\ km/s < FWHM(H\beta) < 8000\ km/s$), $B1^{+}$ ($8000\ km/s < FWHM(H\beta) < 12\ 000\ km/s$) and $B1^{++}$ ($12\ 000\ km/s < FWHM(H\beta) < 16\ 000\ km/s$). $A1$, $A2$, $B1$ and $B1^{+}$ appear to be the most populated quadrants, while $A3$ and $B1^{++}$ are less populated. In recent years, more quasars of $A4$ spectral type and of a $B2$ quadrant ($4000\ km/s < FWHM(H\beta) < 8000\ km/s$ and $0.5 < R_{FeII} < 1.0$)

have also been found. Sparse outliers remain in other 4DE1 regions.
Composite median spectra can be obtained for each spectral type, in order to have a better understanding of the main differences between these quasar classes. Fig. 4.1 (right) shows a comparison of composite spectra in the optical range 4200-5700Å for the quasar sample of Fig. 4.1 (left). The main differences between populations A and B are evident. In particular, moving from $A3$ towards $B1^{+}$ sources, the strength of Fe II emission around 4570 Å decreases and the $H\beta$ line becomes broader. The composite spectrum of Narrow Line Seyfert I galaxies (NLS1, a particular population A subclass that will be discussed in Section 5.4) does not show significant differences between $A1$ and $A2$ quadrants and is also represented in Fig. 4.1 (right). Finally, Fig. 4.2 shows the composite $H\beta$ line profiles and the different best-fitting functions mentioned before.

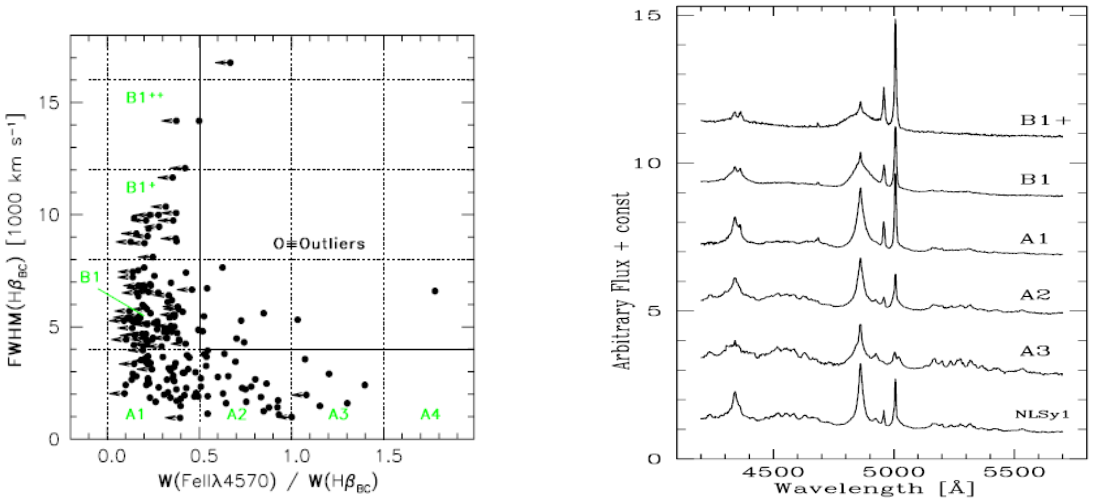

Figure 4.1: Left: Optical plane of the 4DE1 diagram showing the different quasar spectral types. The points with horizontal arrows represent R_{FeII} upper limits, in particular in population B sources which have a weaker Fe II emission. Right: Composite median spectra for the different spectral types, in the optical range 4200-5700 Å of the quasar rest frame. In particular, the Fe II blend at 4570 Å, the $H\beta$ Balmer line and the narrow forbidden lines of [O III] $\lambda\lambda 4959, 5007$ are well visible (Sulentic et al. 2002).

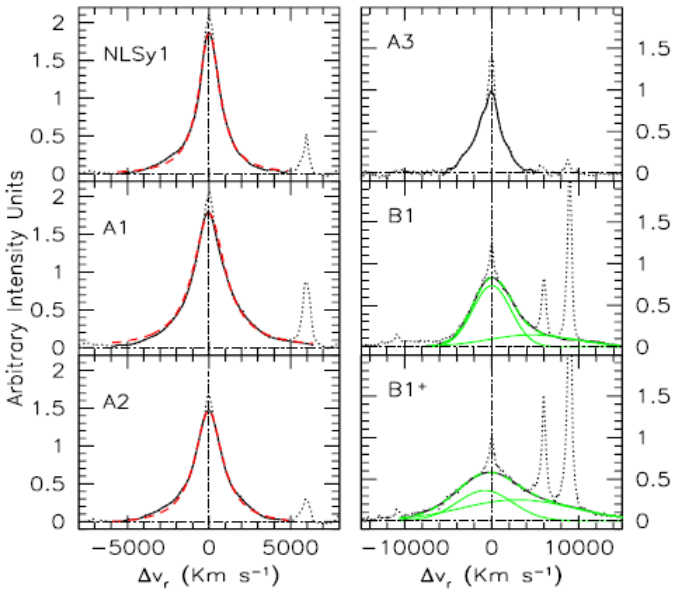

Figure 4.2: Composite $H\beta$ line profiles for the different spectral types of Fig. 4.1 sample. The line profiles are obtained after subtraction of the continuum emission, Fe II λ4570, [O III] $\lambda\lambda 4959, 5007$, He II λ4686 and $H\beta$ narrow line component. A red dashed curve represents a Lorentzian fit, a green dashed curve a double Gaussian model. The line profile for $A3$ spectral type was not fitted because it was based on only five sources (Sulentic et al. 2002).

The presence of a disk wind component in population A sources likely inhibits the radio jets, in fact these quasars are mainly radio-quiet (Zamfir et al. 2009). The majority (78%) of radio-loud quasars belong to population B; almost all have $R_{FeII} < 0.5$, show red asymmetries in broad line profiles and redshifted C IV lines, and lack a soft X-ray excess, while having a higher hard X-ray emission. The position of the different radio-loud morphologies in the 4DE1 optical plane is shown in Fig. 4.3: core-dominated sources are placed at rather smaller $FWHM(H\beta)$ and larger R_{FeII} than the FR II lobe-dominated ones (Fig. 4.3 left panel), and show a higher C IV line redshift (Fig. 4.3 right): as mentioned in Chapter 2, these features are interpreted in terms of a different orientation.
The fact that RL quasars occupy a more restricted region in the 4DE1 diagram, compared to the RQ majority, means that the two classes cannot be completely unified: several factors, both environmental and intrinsic, have been proposed in order to explain the difference.
Environmental factors are suggested by the fact that bright jets are usually observed in elliptical galaxies and not in spirals, where a jet would be decelerated in the gas-rich environment: RL quasars are usually found in massive ellipticals. An important intrinsic factor instead is the BH spin: a more intense radio loudness is thought to be related to a higher spin, which is likely to be found in massive elliptical galaxies (Chapter 6 of Netzer 2013).

Moreover, radio activity could be a relatively shorter (10^7-10^8 years) recurrent phase in AGN life, in fact some observations of weak diffuse radio emission are consistent with a previous radio activity. A radio-loud quasar may undergo alternate phases of quiescence and activity. However, it is not clear whether there is a BH mass threshold that gives rise to radio loudness, which may imply an evolutionary connection between some radio-quiet sources and radio-loud ones (Sulentic et al. 2014, and references therein).

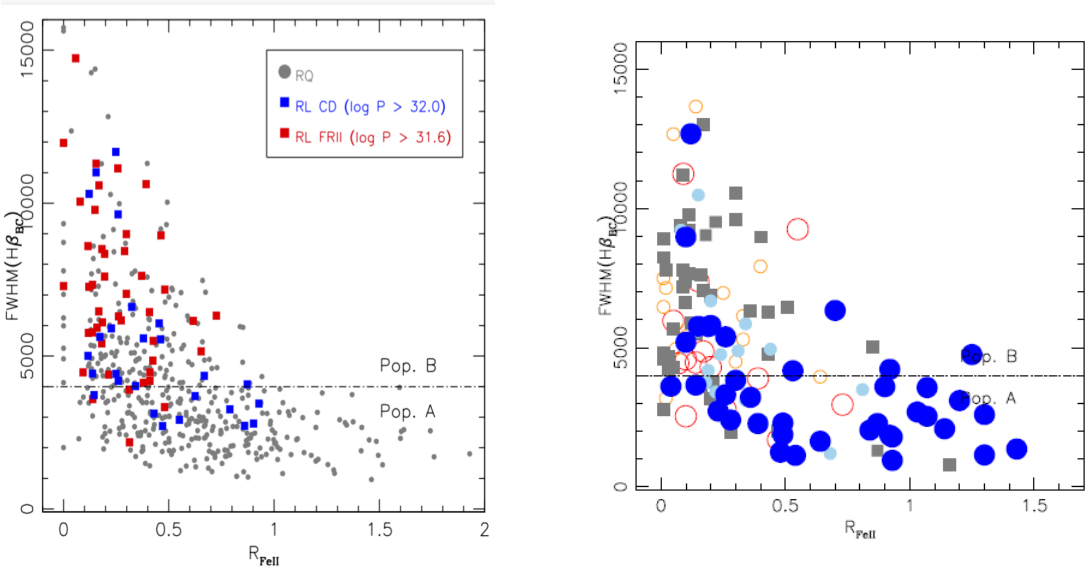

Figure 4.3: Left: Optical plane of 4DE1 diagram showing the different distributions of radio-quiet, core-dominated radio-loud and FR II radio-loud quasars. The horizontal line corresponds to the boundary between populations A and B (Sulentic et al. 2015). Right: 4DE1 optical plane showing how the C IV line shift varies along the quasar sequence. Large blue filled circles correspond to a high blueshift ($\Delta v_r < -1000\ km/s$, with a preference for RQ population A), small light-blue circles to a slight blueshift ($-1000\ km/s \leq \Delta v_r < -200\ km/s$). Grey squares represent quasars with no significant shift ($-200\ km/s \leq \Delta v_r \leq 200\ km/s$, with a preference for RQ population B). Small orange open circles correspond to a slight redshift ($200\ km/s < \Delta v_r \leq 1000\ km/s$, mainly FR II RL), and large red open circles to a high redshift ($\Delta v_r > 1000\ km/s$, mainly core-dominated RL) (Sulentic et al. 2014).

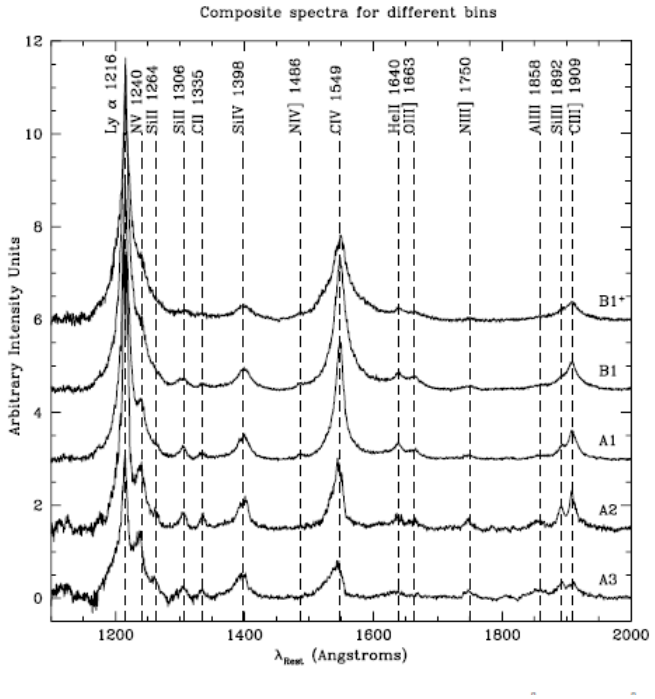

Figure 4.4: Composite UV spectra (in the range 1150-1950 Å of quasar rest frame) for the different quasar spectral types. The spectra are obtained after subtraction of continuum and Fe II emission. In particular, the C IV line at 1549 Å shows an evident transition from a blueshifted profile of population A to a substantially symmetric profile of population B (Bachev et al. 2004).

4.2 THE EDDINGTON RATIO AS THE FUNDAMENTAL DRIVER OF THE SEQUENCE

Past and recent studies found out that the fundamental parameter that drives the quasar sequence in the 4DE1 optical plane is the Eddington ratio L_{bol}/L_{edd}, proportional to the ratio of luminosity to BH mass, convolved with the line of sight orientation (e.g. Marziani et al. 2001, Shen & Ho 2014). For example, a nearly face-on orientation would favour the same features of a high L_{bol}/L_{edd}: a more intense soft X-ray excess, smaller $FWHM(H\beta)$ and stronger Fe II lines.
Quasar parameters correlate better with L/M_{BH} than with M_{BH} alone. Moreover, since populations A and B have the same luminosity distributions, population A sources are expected to have smaller BH masses and higher L/M_{BH} than population B. So the Eddington ratio increases when moving from high $FWHM(H\beta)$ sources, in the upper left part of 4DE1 diagram, towards smaller $FWHM(H\beta)$ sources, in the lower right part: that is, from population B towards extreme population A sources.
However, the difference may not be so large, if proper correction in considering $H\beta$ $FWHM$ an estimator of M_{BH} is taken into account. In fact, the redshifted side of $H\beta$ line profiles in population B quasars (shown in Fig. 4.2) could be related to a radial motion, an inflow, at the inner edge of the BLR (Zamfir et al. 2009); so it is

better to rely mainly on the unshifted component in estimating the BH mass. After the correction, population B BH mass would decrease and the Eddington ratio increases, reducing the difference between populations A and B.
The $FWHM(H\beta) = 4000\ km/s$ boundary between the two populations corresponds to $L_{bol}/L_{edd} \approx 0.2 \mp 0.1$ for $M_{BH} \approx 10^8\ M_\odot$ (Sulentic et al. 2014, and references therein), which is consistent with a turning point in the structure of the accretion disk. The features in the broad line profiles of population B are in accordance with the model of the geometrically thin disk whose kinematics is dominated by Keplerian rotation, which is indeed the structure that is expected to form in the case of low accretion rate. Instead, when L_{bol}/L_{edd} becomes larger than 0.2-0.3, the disk is expected to become geometrically thick (slim disk) and to be able to produce a steep soft X-ray spectrum and a radiation driven wind. Population A quasars show spectroscopic properties that are consistent with a slim disk structure. So the distinction between populations A and B may correspond to a real physical transition in the structure of the BLR (Sulentic et al. 2000, Sulentic et al. 2014).
All these considerations have suggested to interpret the trend in 4DE1 optical plane as an evolutionary sequence, with highly accreting population A quasars as the youngest ones (in particular Narrow Line Seyfert I galaxies) and low accreting population B as a more evolved population (Sulentic et al. 2000, Krongold et al. 2001, Sulentic et al. 2014).

CHAPTER 5

MORPHOLOGICAL PROPERTIES OF QUASAR HOSTS

The analysis of the morphology of quasar hosts and their environment is possible only at low redshift, because a high spatial resolution and a good PSF model for the central source are needed in order to correctly subtract the light of the nucleus from the host galaxy. The higher the luminosity of the quasar compared to the host contribution, the more difficult the nuclear point subtraction becomes; the situation is quite improved in the near-infrared, where morphological studies of quasar hosts up to $z \approx 2$ are possible. The analysis of higher redshift quasar hosts could become possible in the next future, thanks to forthcoming telescopes such as the James Webb Space Telescope (JWST) and the European Extremely Large Telescope (E-ELT).

5.1 PHOTOMETRICAL DECOMPOSITION

The photometrical decomposition of a quasar and its host is obtained describing the central point source with the PSF (Point Spread Function) from uniformly distributed stars in the local field around the quasar, and the galaxy with a surface brightness profile: an example is shown in Fig. 5.1.
One of the most important photometric model for a spheroid system (bulge or elliptical galaxy) is the De Vaucouleurs' law:

$$I(r) = I_e e^{-7.67[(r/r_e)^{1/4}-1]} \iff \mu(r) = \mu_e + 8.325[(r/r_e)^{1/4} - 1] \tag{5.1}$$

where the surface brightness is in linear units and in $mag\ arcsec^{-2}$, respectively, and with r_e the effective radius (the radius that contains half of the galaxy light) and $\mu_e = -2.5 log I_e$ the surface brightness at r_e.
A disk component is usually described with an exponential law:

$$I(r) = I_0 e^{-r/h} \iff \mu(r) = \mu_0 + 1.086(r/h) \tag{5.2}$$

with h the exponential scale length and $\mu_0 = -2.5 log I_0$ the central surface brightness.
The generalization of the De Vaucouleurs' law is achieved through the Sérsic model:

$$I(r) = I_e e^{-b_n[(r/r_e)^{1/n}-1]} \iff \mu(r) = \mu_e + 1.086 b_n[(r/r_e)^{1/n} - 1] \tag{5.3}$$

with $b_n = 2n - 0.324$ determined in order to have r_e as the effective radius. The Sérsic index n varies from $n \approx 4$ (De Vaucouleurs profile) in early-type galaxies towards $n \approx 1$ in late-type ones: $n \approx 2.5$ can be considered a boundary between disk-dominated (late-type) and bulge-dominated (early-type) systems.

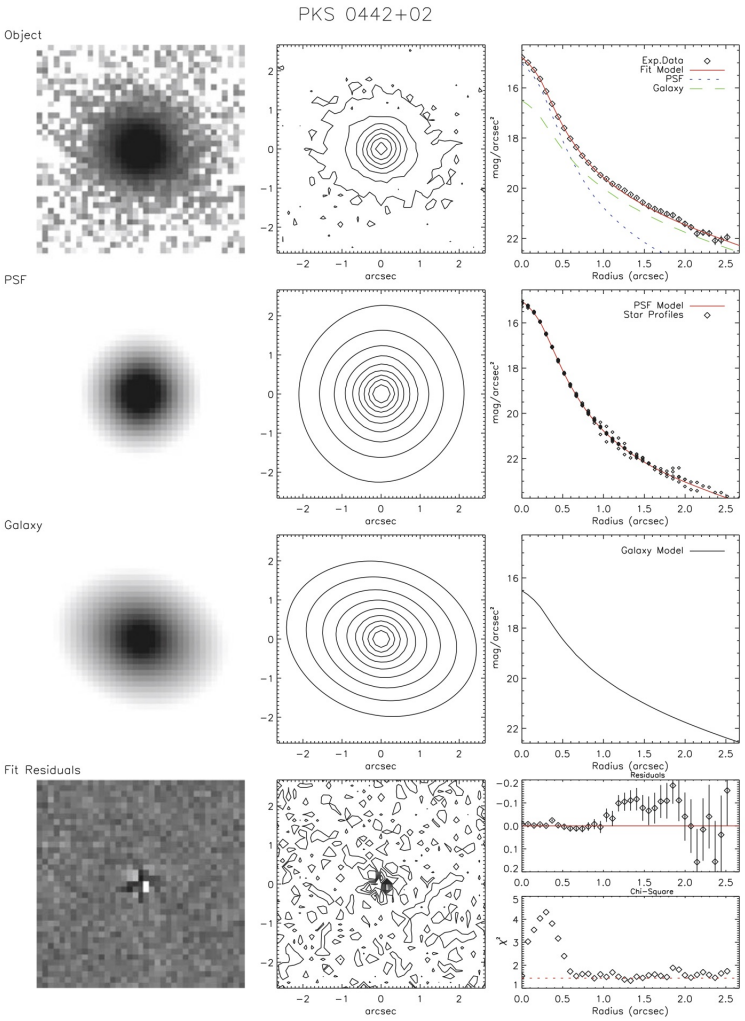

Figure 5.1: Example of quasar photometrical decomposition into nucleus and host. The first row represents the total object, the second one the nuclear point source described by the PSF model, the third row the host galaxy. In each row, the image (left), the contour lines of equal surface brightness (middle), and the average surface brightness profile (right) are shown. The last row represents the residuals after the fitting (Chapter 7 of D'Onofrio et al. 2012).

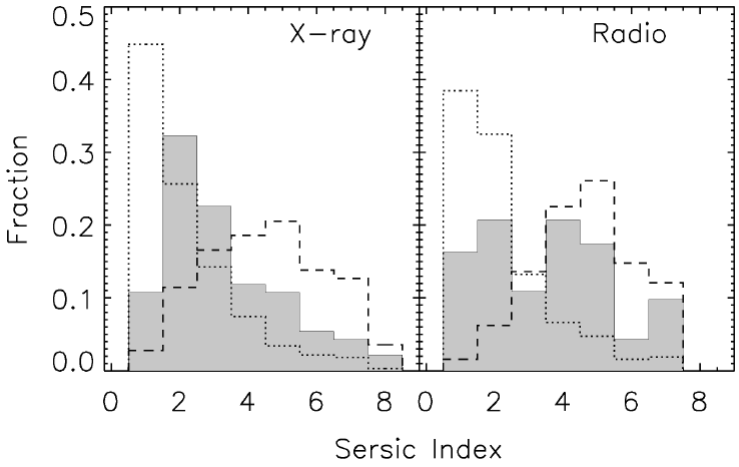

Figure 5.2: Distribution of the Sérsic index for X-ray-selected and radio-selected quasars (grey area, left and right respectively) compared with that of corresponding inactive galaxies, divided into early type (dashed line) and late-type (dotted line). Both quasar samples span a large range of morphological types. The apparent bimodality in the radio samples is probably due to contamination from star-forming galaxies, which usually have disk-dominated morphologies (Gabor et al. 2009).

5.2 MORPHOLOGY, COLOUR AND ENVIRONMENT

At low redshift, except for particularly perturbed systems, the morphological types of quasar hosts appear very similar to those of inactive galaxies at the same redshift, varying from bulge-dominated to disk-dominated: assuming a Sérsic brightness profile, the Sérsic index appears to span a broad range of values, as shown in Fig. 5.2. Radio-quiet high luminosity quasars are found both in coreless elliptical (elliptical galaxies whose surface brightness profile follows a power-law function in the nuclear region) and disk galaxies, while radio-loud ones prefer massive core ellipticals (elliptical galaxies whose surface brightness profile is flattened in the nuclear region with respect to the power-law profile of the outer region). Low luminosity AGNs (the Seyfert galaxy ones) are usually found in spiral and disk galaxies; bars and other asymmetric structures are also present, but not more frequently than in the corresponding inactive galaxies. Both in active and inactive galaxies, there is a slight increase in luminosity with redshift due to the evolution of the stellar population (Gabor et al. 2009, Falomo et al. 2014).
Usually disk-dominated quasar hosts have similar colours to that of the corresponding inactive galaxies, while the colours of bulge-dominated ones are bluer (Bettoni et al. 2015): this fact may indicate a relatively young or intermediate-age stellar population. In a colour-magnitude diagram for galaxies, in fact, quasar hosts lie in the region called the 'green valley', between the 'red sequence' of massive bulge-dominated galaxies with old stellar population, and the 'blue cloud' of small and intermediate mass galaxies with young stellar population.
An example is provided in Fig. 5.3, which represents a sample of X-ray-selected quasars at $z \lesssim 2$ in the diagram $B-V$ colour against absolute magnitude in B-band M_B: about

60% of quasars are located in the region with $18 \leq M_B \leq -21.5$ and $0.3 \leq B-V \leq 0.9$, with the boundary between the red sequence and the blue cloud set at $B - V = 0.6$. This fact has suggested that quasar hosts in the green valley may be in a transition phase from the blue cloud to the red sequence, because of the quenching of star formation due to AGN activity (Pović et al. 2012).
At low and intermediate luminosity, statistical comparison of the environment of inactive galaxies and quasar hosts has shown that both the probability of having a near companion and the fraction of disturbed morphology are usually similar: these active galaxies do not undergo strong interaction effects more frequently than inactive galaxies at the same redshift and luminosity (Bettoni et al. 2015, Gabor et al. 2009). Instead, when moving to high-luminosity quasars ($L_{bol} \approx 10^{47}$ - 10^{48} erg/s), the fraction of perturbed systems and the probability of having bright near companions increase. At this high luminosity, evidence of strong interactions with close companions and merging features are found also in low redshift nearby quasars: the HST images shown in Fig. 5.5 provide a clear example.
In nearby inactive galaxies, the BH mass appears to be well correlated with the stellar velocity dispersion, the mass and the luminosity of the bulge component, as shown in Fig. 5.4. This is considered a hint of a coevolution between the galaxy, or at least its bulge component, and the central black hole (see Kormendy & Ho 2013 for an appropriate discussion). Instead, galaxies with pseudobulges do not follow the same correlation, deviating mainly below the line (Narrow-Line Seyfert I sources are thought to be preferentially hosted in these systems, see Section 5.4).
In the relationship between BH mass and host absolute magnitude, the majority of quasar hosts lie below the relation, in the sense that they appear more luminous than expected at a given BH mass, and show a larger scatter for a fixed luminosity. In recent studies (Bettoni et al. 2015, Falomo et al. 2014) this fact is interpreted as due to a significant disk component that is not correlated with BH mass: indeed, if in the diagram only the absolute magnitude of the bulge component is considered, the correlation is improved. This indicates that a careful morphological and photometrical decomposition of a significant fraction of low redshift quasar hosts needs to take into account both a bulge and a disk component.

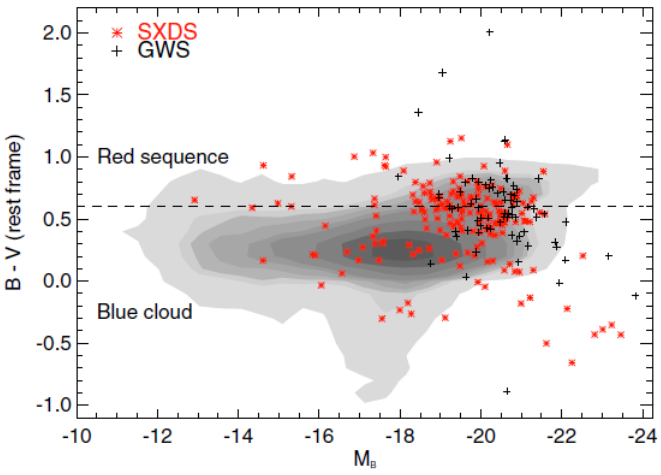

Figure 5.3: Colour-magnitude diagram ($B-V$ colour against absolute magnitude in B-band M_B) for X-ray-selected quasars at $z \lesssim 2$. Different symbols represent the data from GWS (Groth-Westphal Strip, black crosses) and from SXDS (Subaru/XMM-Newton Deep Survey, red stars). The area occupied by inactive galaxies is also shown for comparison, with darker grey corresponding to higher density of sources and lighter grey to a lower density. The horizontal line at $B-V=0.6$ represents the boundary between the blue cloud and the red sequence (Pović et al. 2012).

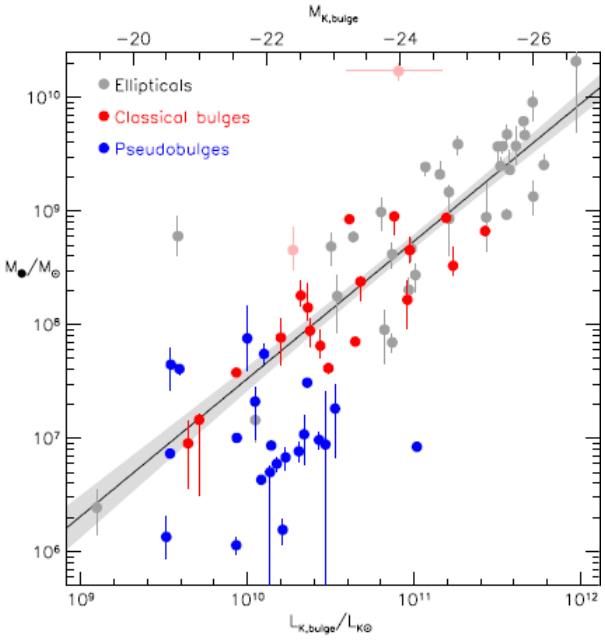

Figure 5.4: Correlation between BH mass and absolute magnitude (or luminosity) in K band of the host bulge component in nearby inactive galaxies. The black line represents the best correlation for ellipticals and classical bulges, the grey shade the 1σ range of error. Pseudobulges are mainly located below the line (see Section 5.4) (Kormendy & Ho 2013).

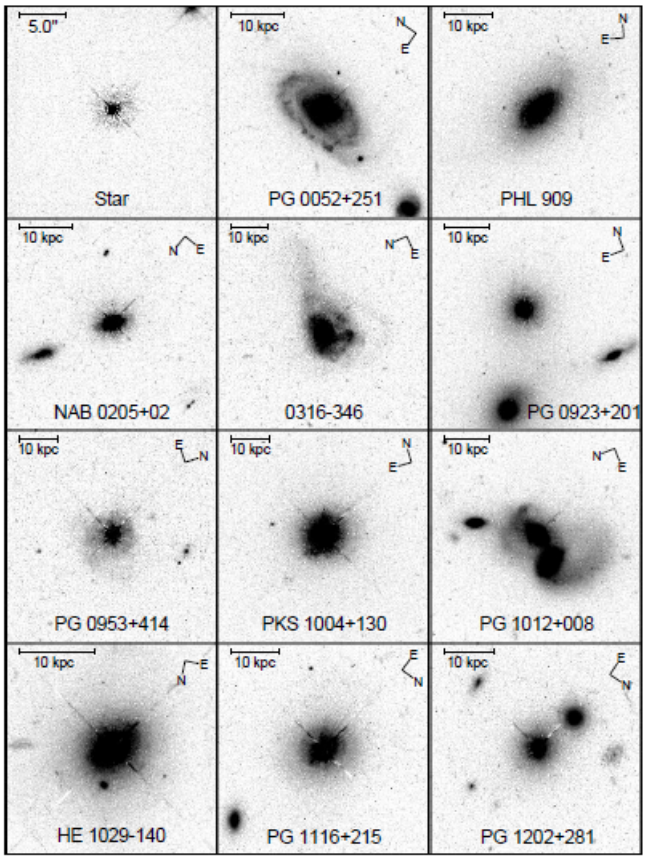

Figure 5.5: Images of some of the most luminous ($M_V < -22.9$) nearby ($z < 0.30$) quasars, obtained with the Wide-Field Camera of HST (Hubble Space Telescope). Strong gravitational interaction features and presence of bright companions are evident (Bahcall et al. 1997).

5.3 TRIGGERING OF AGN ACTIVITY

The most important idea that was first proposed to explain the triggering of AGN activity involved major mergers and strong gravitational interactions with nearby galaxies: these processes destroy the original galaxy morphology and bring gas to the center leading to activation and growth of the BH. Observations and systematic studies of large AGN samples, with different luminosities and redshift up to $z \approx 2$, have led to the conclusion that this is indeed the situation of high-luminosity quasars, but is not the dominant mechanism for low-intermediate luminosity quasars.
In the latter case, a significant fraction of quasar hosts appears to be disk-dominated, but disk-dominated systems would be destroyed in a major merger; moreover, the host colours and morphological types are very similar to those of inactive galaxies, and there is also no significant difference in their environment. Those features indicate that, at low redshift and low-intermediate luminosity, AGN activity is mainly triggered by minor interactions or secular processes due to dynamical instability inside the galaxy, with little effect on the stellar population and on the galaxy global structure (Gabor

et al. 2008, Chapter 8 of Netzer 2013).

5.4 NARROW-LINE SEYFERT I GALAXIES

NLS1 (Narrow-Line Seyfert I Galaxies) are a subclass of Seyfert I galaxies that show particular features compared with the other members of the class: $FWHM(H\beta) \leq 2000\ km/s$, some of them with very strong Fe II emission, steep X-ray spectra and a high soft X-ray excess. These properties place a large fraction of NLS1 galaxies at the population A extreme of the quasar sequence in the 4DE1 diagram, suggesting that they represent AGN with the highest Eddington ratio (Krongold et al. 2001).
A larger Eddington ratio, and so L/M_{BH}, combined with a similar luminosity distribution compared with the other Seyfert I galaxies, implies a smaller black hole mass. This is confirmed by morphological analysis, which found out that NLS1 usually have smaller sizes ($r_e \leq 2\ kpc$) than broad line Seyfert I, and smaller galaxies are expected to host less massive black holes. Moreover, morphological studies also found out that, fitting the bulge component with a Sèrsic profiles, a significant fraction of NLS1 appears to have a Sérsic index $n \leq 2.2$, meaning that the bulge component is rather a pseudobulge than a classical bulge (which is instead found in broad line Seyfert I) (Mathur et al. 2012).
Pseudobulges are different from classical bulges in the sense that they show disk-like properties: a larger contribution of ordered velocity compared to the velocity dispersion. In addition, nuclear bars or other asymmetric structures are present. As mentioned, they are associated with surface brightness profiles that do not follow De Vaucouleurs law, and are instead best fitted with a Sèrsic profiles with $n \lesssim 2$. Pseudobulges show also a younger stellar population than classical bulges. While classical bulges follow a clear correlation between BH mass and bulge luminosity, with more massive black holes hosted in more luminous bulges, pseudobulges lie below the relation (see Fig. 5.4), and this is what is found for NLS1 galaxies. The different structural and kinematic properties of pseudobulges suggests a formation process different from the merger mechanism that leads to classical bulges: pseudobulges probably evolve through slower secular processes and minor interactions.
The analysis of the environment of NLS1 has pointed out that these active galaxies do not show signs of present or past merging events, and appear to have less companions than inactive galaxies with similar size and redshift. Their pseudobulges may be still in an early evolutionary phase, as suggested also by observations of young stellar or even star-forming population. Their black hole masses are smaller ($M_{BH} \approx 10^6$-$10^7\ M_\odot$) and still growing with a high Eddington ratio. So NLS1 galaxies may be interpreted as AGNs in the earliest phase of evolution.

CHAPTER 6

A FUTURE PERSPECTIVE: A LINK BETWEEN 4DE1 AND HOST MORPHOLOGY

The majority of morphological studies on quasar hosts has so far analysed AGN samples without distinction about the location in the 4DE1 sequence. However, given the possible interpretation of the 4DE1 sequence as an evolutionary trend, it would be interesting to study the host morphology in samples restricted to specific regions of the 4DE1 diagram, in order to understand whether quasars with a certain range of black hole mass values show a preference for particular morphological features, and how the Eddington ratio could be influenced by the circumgalactic environment.
The studies focused on NLS1 galaxies have shown that these highest-accreting (extreme population A) AGN are usually hosted in pseudobulges that are still growing by secular processes and do not show signs of strong interaction with the surrounding environment. What are instead the host features of intermediate population A quasars, or of the lowest-accreting population B sources? Does the mass and accretion rate sequence in 4DE1 correspond also to a change in morphological properties? Systematic studies on morphological types and colours, presence of asymmetric structures and environmental features (excess or defect of companions, frequency of interacting systems) need to be carried out for each restricted region along the quasar sequence (for example limiting R_{FeII} and $FWHM(H\beta)$ according to the definition of spectral types).
For such studies, it is better to rely on homogeneous samples of type I AGN, from surveys where images are obtained with the same filter system and spectroscopic data have similar quality and resolution. An optical survey should also be matched with surveys at other wavelengths in order to have a better understanding of the properties of the sample: in particular, a corresponding radio survey is important for the distinction between radio-loud and radio-quiet quasars. Moreover, an appropriate redshift limit should be considered, in order to allow both a reliable morphological decomposition of the host galaxy and the detailed analysis of $H\beta$ line and its surrounding spectral region (and therefore the correct knowledge of the source position in the 4DE1 sequence). The latter is due to the fact that quasars with a higher redshift show a $H\beta$ line that is more shifted towards larger wavelengths (with all the other spectral lines) and eventually gets out of the wavelength range covered by the survey.
A large quasar sample can be provided by the Sloan Digital Sky Survey (SDSS) data releases, whose objects are matched with the FIRST [1] radio survey. If a data release before DR9 is used, the upper limit wavelength of the spectral range is 9200 Å. Therefore spectroscopic analysis should be limited at $z \lesssim 0.9$ (at this value the $H\beta$ line is found at 9200 Å), or better at $z \lesssim 0.8$ (the 5130 Å Fe II blend is found at

[1] Faint Images of the Radio Sky at Twenty cm

9200 Å) in order to estimate correctly the continuum and Fe II emissions that have to be subtracted from the $H\beta$ line. Instead, in DR9 and further data releases, the BOSS [2] spectrograph extended the wavelength range up to 10 400 Å and the redshift limit can become $z \lesssim 1.1$, or better $z \lesssim 1.0$. However, a reliable host morphological analysis of such a SDSS sample requires a more restricted redshift limit, about $z \lesssim 0.2$. An exception is represented by the SDSS images of Stripe 82 (a particular region of the sky in the celestial equator), which are two magnitudes deeper than normal SDSS images: in this case, host morphological analysis is possible up to $z \approx 0.5$-0.6 (e.g. Falomo et al. 2014).
Therefore, in order to search a reliable connection between 4DE1 properties and host morphology using a SDSS-based sample, the analysis is limited at $z \lesssim 0.2$. Nonetheless, the results could be important and could represent a term of comparison for future surveys with telescopes that will allow a deeper analysis of host morphology.
Turning towards other surveys, an AGN sample could be provided by the Cosmic Evolution Survey (COSMOS), whose optical images are obtained with HST Advanced Camera for Surveys (ACS) and complemented with observations at different wavelengths with other telescopes, for example the VLA [3] in the radio domain, XMM/Newton [4] and Chandra at X-ray, Herschel and Spitzer in the infrared. COSMOS spectra are also obtained with different instruments, for example VIMOS of VLT [5] and IMACS [6] of Magellan Telescope, which cover a similar wavelength range to that of SDSS. With the FMOS [7] of the Subaru Telescope, this limit could be extended up to 18 000 Å, allowing the analysis of $H\beta$ line and surroundings up to $z \approx 2.5$. Host morphological analysis of COSMOS data is possible up to about $z \approx 1$ thanks to HST high angular resolution. In this case, it would be interesting to consider first all quasars of the same spectral type and different z together, and then to divide the sources in redshift bins in order to understand whether there is a change with redshift in the range $z \lesssim 1$.

A particular possibility regards the morphological analysis of population B quasars located in the region of 4DE1 diagram where radio-loud sources are more frequent, between 4000 $km/s \leq FWHM(H\beta) \leq 8000$ km/s and $0.0 \leq R_{FeII} \leq 0.5$ (the $B1$ spectral type). In this region, an SDSS-FIRST-based sample (e. g. Zamfir et al. 2008) of RQ and RL quasars that share the same optical spectroscopic properties and have similar BH masses, luminosities and Eddington ratios ($M_{BH} \approx 10^{8.5} M_{\odot}$, $L_{bol} \approx 10^{45.5}$ erg/s and $L_{bol}/L_{edd} \approx 0.1$) could be considered. It would be interesting to know whether there are systematic differences between the hosts of these quasars, which are very similar except for the different radio-loudness. This study would provide new information for the still-open question about the main driver of radio-loudness, for which both intrinsic nuclear difference (BH spin, rotation of the inner accretion disk, a mass threshold, magnetic field) and environmental effects (preference for gas-poor

[2] Baryon Oscillation Spectroscopic Survey
[3] Karl Jansky Very Large Array
[4] X-ray Multi-Mirror Mission
[5] Visible Multi-Object Spectrograph, Very Large Telescope
[6] Inamori Magellan Areal Camera and Spectrograph
[7] Fibre-fed Multi-Object Spectrograph

galaxies and core ellipticals) have been proposed.
Fig. 6.1 shows an example of three different sources, at redshift $z < 0.2$ and classified in the $B1$ spectral type according to Zamfir et al. 2008: a RQ, a RL lobe-dominated and a RL core-dominated. Their SDSS optical spectra and images are complemented with the FIRST radio maps that show the clear distinction between radio-loud and radio-quiet. In this example, the RL lobe-dominated source appears to have more near bright companions than the RQ one. The spectacular strong interacting or perturbed systems of Fig. 5.5 are also found to be radio-loud. However, these are only a few examples that have no statistical validity. A systematic study is needed in order to find out whether these are only particular cases or whether nearby RL quasars show really a preference for more bright companions and perturbed systems with respect to RQ sources. If the latter case turned out to be statistically valid, it would represent a further hint that an increase of the BH spin and/or of the accretion rate above a certain mass threshold, consequence of a major merger or of a strong environmental perturbation, could trigger radio-loudness.
In order to carry out a more accurate analysis, a strong interacting system should be defined on more quantitative criteria than the simple visual examination of the images. For example, it could be defined on the basis of the distortion in the contour lines of equal surface brightness. Moreover, a maximum limit in the projected separation and in the magnitude difference could be adopted. The quasar host galaxy and its companion can be considered as undergoing a strong interaction if their redshifts are about the same, their projected separation is less than 30-40 kpc at that z, and their difference in apparent magnitude is within 2-3 mag. However, the redshifts of the companions are not always available, and therefore in the general case only a statistical analysis of the potential interacting companions is possible. Precise criteria in the general case could be defined with the help of studies of simulations of interacting systems (e.g. Holincheck et al. 2016).
The SDSS sample, at $z \lesssim 0.2$ and restricted to $B1$ spectral type with BH mass, luminosity and Eddington ratio values as mentioned before, represents an appropriate sample for such an analysis. One of the main advantages of such a sample would be a valid determination of the radio morphology thanks to the matching with the FIRST survey and the low redshift limit. Thanks to the $z \lesssim 0.2$ limit, a reliable knowledge of the redshift of the companions is also more probable, allowing to determine whether they are really possible interacting companions. Finally, the restriction of the analysis only to $B1$ quadrant allows a more statistically valid comparison between RL and RQ properties, because RL sources represent a more significant part of the sample (about 30%) with respect to a sample of all spectral types together (8%).

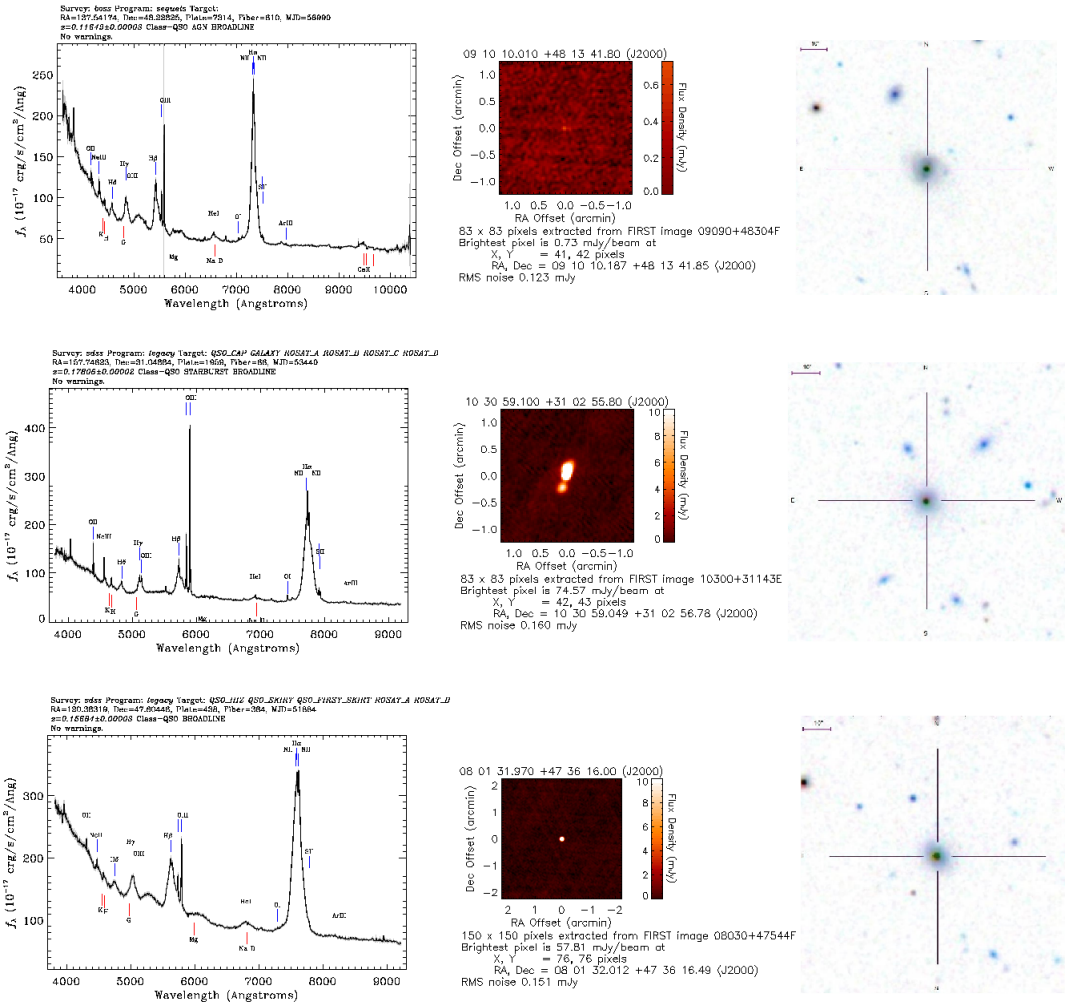

Figure 6.1: Example of a RQ (top), a RL lobe-dominated (middle) and a RL core-dominated (bottom) quasars at $z < 0.2$. For each source, the SDSS optical spectrum, the FIRST radio map and the SDSS optical image are shown (http://skyserver.sdss.org/dr13/en/home.aspx, http://sundog.stsci.edu/).

CHAPTER 7

CONCLUSION

Quasars are among the most energetic and distant objects that can be observed in the Universe. The study of these sources is important in order to understand the role of nuclear activity in galaxy evolution. Quasars show an intense energy emission that span almost all the domains of the electromagnetic spectrum. This emission is due both to thermal and nonthermal processes and arises from distinct quasar components located at different distances from the central black hole. The nuclear activity can have an important influence on the evolution of the host galaxy through different feedback mechanisms.

While all quasars share the same basic mechanism of accretion of gas onto a supermassive black hole, the great variety of spectroscopic properties reveals that the accretion can occur in very different modes due to intrinsic diversity. In particular, the accretion disk that emits the optical-UV continuum can change shape from a thin to a slim disk when the Eddington ratio increases beyond the value $L_{bol}/L_{edd} \approx 0.2$-$0.3$. The 4DE1 diagram offers a possible way to organize the various spectroscopic properties and leads to the distinction of the two different quasar populations A and B. The 4DE1 sequence may be interpreted as an evolutionary path from the highest-accreting NLS1 nuclei of relatively small mass, to the more massive population B sources.

Apart from the great variety of spectroscopic features, quasar are hosted in galaxies that also show a large diversity of morphologies, colours and environments. A detailed analysis of both spectroscopic and host morphological features is possible only at low redshift, although some properties can be extended also to high-z sources. Future systematic morphological studies need to be carried out for each quasar spectral type in the 4DE1 sequence, in order to understand the possible connections between the intrinsic properties of the nucleus (spin, mass, accretion rate) and the features of the host galaxy. These studies could be important in the search for an answer to some still-open questions, such as the nature of the radio-loud/radio-quiet difference.

REFERENCES

Antonucci R., 1993, "Unified models for active galactic nuclei and quasars", *Annual review of astronomy and astrophysics*, Vol. 31, pp. 473-521

Bachev, R.; Marziani, P.; Sulentic, J. W.; Zamanov, R.; Calvani, M.; Dultzin-Hacyan, D., 2004, "Average Ultraviolet Quasar Spectra in the Context of Eigenvector 1: A Baldwin Effect Governed by the Eddington Ratio?", *The Astrophysical Journal*, Vol. 617, pp. 171-183

Bahcall, J. N.; Kirhakos, S.; Saxe, D. H.; Schneider, D. P., 1997, "Hubble Space Telescope Images of a Sample of 20 Nearby Luminous Quasars", *The Astrophysical Journal*, Vol. 479, pp. 642-658

Bensch, K.; del Olmo, A.; Sulentic, J.; Perea, J.; Marziani, P, 2015, "Measures of the Soft X-ray Excess as an Eigenvector 1 Parameter for Active Galactic Nuclei", *Journal of Astrophysics and Astronomy*, Vol. 36, pp.467-474

Bettoni, D.; Falomo, R.; Kotilainen, J. K.; Karhunen, K.; Uslenghi, M., 2015, "Low-redshift quasars in the SDSS Stripe 82. Host galaxy colours and close environment", *Monthly Notices of the Royal Astronomical Society*, Vol. 454, pp.4103-4113

Collin-Souffrin, S.; Lasota, J.-P., 1988, "The broad-line region of active galactic nuclei revisited", *Publications of the Astronomical Society of the Pacific*, Vol. 100, pp. 1041-1050

D'Onofrio, M.; Marziani, P.; Sulentic, J. W. Editors, 2012, *Fifty years of quasars. From early observations and ideas to future research*, Springer-Verlag Berlin Heidelberg, Chaps. 3 and 6

Dultzin-Hacyan, D.; Krongold, Y.; Fuentes-Guridi, I.; Marziani, P., 1999, "The Close Environment of Seyfert Galaxies and Its Implication for Unification Models", *The Astrophysical Journal*, Vol. 513, pp. L111-L114

Falomo, R.; Bettoni, D.; Karhunen, K.; Kotilainen, J. K.; Uslenghi, M., 2014, "Low-redshift quasars in the Sloan Digital Sky Survey Stripe 82. The host galaxies", *Monthly Notices of the Royal Astronomical Society*, Vol. 440, pp.476-493

Fanaroff B. L.; Riley J. M., 1974, "The morphology of extragalactic radio sources of high and low luminosity", *Monthly Notices of the Royal Astronomical Society*, Vol. 167, pp. 31-36

Gabor, J. M.; Impey, C. D.; Jahnke, K.; Simmons, B. D.; Trump, J. R.; Koekemoer, A. M.; Brusa, M.; Cappelluti, N.; Schinnerer, E.; Smolčić, V.; and coauthors, 2009, "Active Galactic Nucleus Host Galaxy Morphologies in COSMOS", *The Astrophysical Journal*, Vol. 691, pp. 705-722

Ghisellini, G.; Tavecchio, F, 2009, "Canonical high-power blazar", *Monthly Notices of the Royal Astronomical Society*, Vol. 397, pp. 985-1002

Gruppioni, C.; Berta, S.; Spinoglio, L.; Pereira-Santaella, M.; Pozzi, F.; Andreani, P.; Bonato, M.; De Zotti, G.; Malkan, M.; Negrello, M.; and coauthors, 2016, "Tracing black hole accretion with SED decomposition and IR lines: from local galaxies to the high-z Universe", *Monthly Notices of the Royal Astronomical Society*, Vol. 458, pp.

4297-4320

Holincheck, A. J.; Wallin, J. F.; Borne, K. ; Fortson, L.; Lintott, C.; Smith, Arfon M.; Bamford, S.; Keel, W. C.; Parrish, M., 2016, "Galaxy Zoo: Mergers - Dynamical models of interacting galaxies", *Monthly Notices of the Royal Astronomical Society*, Vol. 459, pp.720-745

Joly, M.; Véron-Cetty, M.; Véron, P., 2008, "Fe II emission in AGN", in "The Nuclear Region, Host Galaxy and Environment of Active Galaxies" (Eds. Erika Benítez, Irene Cruz-González, and Yair Krongold), *Revista Mexicana de Astronomía y Astrofísica (Serie de Conferencias)*, Vol. 32, pp. 59-61

Kellermann, K. I.; Sramek, R.; Schmidt, M.; Shaffer, D. B.; Green, R., 1989, "VLA observations of objects in the Palomar Bright Quasar Survey", *The Astronomical Journal*, Vol. 98, pp. 1195-1207

Kormendy, J.; Ho, L. C., 2013, "Coevolution (Or Not) of Supermassive Black Holes and Host Galaxies", *Annual Review of Astronomy and Astrophysics*, Vol. 51, pp. 511-653

Krongold, Y.; Dultzin-Hacyan, D.; Marziani, P., 2001, "Host Galaxies and Circumgalactic Environment of "Narrow Line" Seyfert 1 Nuclei", *The Astronomical Journal*, Vol. 121, pp. 702-709

Laor, A., 2003, "Some Comments related to AGN Radio Loudness", astro-ph/0312417

Marziani, P.; Sulentic, J. W.; Dultzin-Hacyan, D.; Calvani, M.; Moles, M., 1996, "Comparative Analysis of the High- and Low-Ionization Lines in the Broad-Line Region of Active Galactic Nuclei", *Astrophysical Journal Supplement*, Vol. 104, p.37

Marziani, P.; Sulentic, J. W.; Zwitter, T.; Dultzin-Hacyan, D.; Calvani, M., 2001, "Searching for the physical drivers of the Eigenvector 1 correlation space", *The Astrophysical Journal*, Vol. 558, pp. 553-560

Marziani P.; Sulentic J. W., 2012, "Estimating black hole masses in quasars using broad optical and UV emission lines", *New Astronomy Reviews*, Vol. 56, pp. 49-63

Marziani, P.; Sulentic, J. W.; Negrete, C. A.; Dultzin, D.; D'Onofrio, M.; Del Olmo, A.; Martinez-Aldama, M. L., 2014, "Low- and high-z highly accreting quasars in the 4D Eigenvector 1 Context", *Astronomical Review*, Vol. 9, pp. 6-25

Mathur, Smita; Fields, Dale; Peterson, Bradley M.; Grupe, Dirk, 2012, "Supermassive Black Holes, Pseudobulges, and the Narrow-line Seyfert 1 Galaxies", *The Astrophysical Journal*, Vol. 754, p. 9

Netzer, H., 2013, *The physics and evolution of active galactic nuclei*, Cambridge University Press, Chaps. 1, 3, 4, 7 and 8

Pović, M.; Sánchez-Portal, M.; Pérez García, A. M.; Bongiovanni, A.; Cepa, J.; Huertas-Company, M.; Lara-López, M. A.; Fernández Lorenzo, M.; Ederoclite, A.; Alfaro, E.; and coauthors, 2012, "AGN- host galaxy connection: morphology and colours of X-ray selected AGN at $z \leq 2$", *Astronomy & Astrophysics*, Vol. 541, p. 23

Proga, D.; Stone, J. M.; Kallman, T. R., 2000, "Dynamics of Line-driven Disk Winds in Active Galactic Nuclei", *The Astrophysical Journal*, Vol. 543, pp. 686-696

Richards, G. T.; Kruczek, N. E.; Gallagher, S. C.; Hall, P. B.; Hewett, P. C.; Leighly, K. M.; Deo, R. P.; Kratzer, R. M.; Shen, Y., 2011, "Unification of luminous type I quasars through C IV emission", *The Astronomical Journal*, Vol. 141, p. 16

Shen, Y.; Ho, L. C., 2014, "The diversity of quasars unified by accretion and orientation", *Nature*, Vol. 513, pp. 210-213

Sulentic, J. W.; Marziani, P.; Dultzin-Hacyan, D., 2000, "Phenomenology of Broad Emission Lines in Active Galactic Nuclei", *Annual Review of Astronomy and Astrophysics*, Vol. 38, pp. 521-571

Sulentic, J. W.; Marziani, P.; Zamanov, R.; Bachev, R.; Calvani, M.; Dultzin-Hacyan, D., 2002, "Average Quasar Spectra in the Context of Eigenvector 1", *The Astrophysical Journal*, Vol. 566, pp. L71-L75

Sulentic, J. W.; Marziani, P.; Dultzin, D.; D'Onofrio, M.; del Olmo, A., 2014, "Fifty Years of Quasars: Physical Insights and Potential for Cosmology", *Journal of Physics: Conference Series*, Vol. 565, Issue 1

Sulentic, J. W.; Martínez-Carballo, M. A.; Marziani, P.; del Olmo, A.; Stirpe, G. M.; Zamfir, S.; Plauchu-Frayn, I., 2015, "3C 57 as an atypical radio-loud quasar: implications for the radio-loud/radio-quiet dichotomy", *Monthly Notices of the Royal Astronomical Society*, Vol. 450, pp.1916-1925

Villarroel, B.; Korn, A. J., 2014, "The different neighbours around Type-1 and Type-2 active galactic nuclei", *Nature Physics*, Vol. 10, pp. 417-420

Zamfir S.; Sulentic J. W.; Marziani P., 2008, "New Insights on the QSO Radio-Loud/Radio-Quiet Dichotomy: SDSS Spectra in the Context of the 4D Eigenvector1 Parameter Space", *Monthly Notices of the Royal Astronomical Society*, Vol. 387, pp. 856-870

Zamfir, S.; Sulentic, J. W.; Marziani, P., 2009, "Characterization of the $H\beta$ Broad Emission Line in Low Redshift SDSS Quasars", *Bulletin of the American Astronomical Society*, Vol. 41, p. 331